Lightning-generated NO_x seen by OMI during NASA's TC^4 experiment

Eric J. Bucsela[1], Kenneth E. Pickering[2], Tabitha L. Huntemann[3], Ronald C. Cohen[4], Anne Perring[4], James F. Gleason[2], Richard J. Blakeslee[5], Rachel I. Albrecht[3], Robert Holzworth[6], James P. Cipriani[3], Dylana Vargas-Navarro[7], Ileana Mora-Segura[7], Alexia Pacheco-Hernández[7], Sadí Laporte-Molina[7]

[1]SRI International,

[2]NASA Goddard Space Flight Center,

[3]University of Maryland,

[4]University of California, Berkeley,

[5]NASA Marshall Space Flight Center,

[6]University of Washington,

[7]Instituto Costarricense de Electricidad

Abstract: We present case studies identifying lightning-generated upper-tropospheric NO_x (LNO_x) observed during NASA's Tropical Composition, Cloud and Climate Coupling Experiment (TC^4) in July and August 2007. In the campaign, DC-8 aircraft missions, flown from Costa Rica, recorded *in situ* NO_2 profiles near active storms and in relatively quiet areas. We combine these TC^4 DC-8 data with satellite data from the Ozone Monitoring Instrument (OMI) to estimate the lightning-generated NO_2 (LNO_2)—above background levels—in the observed OMI NO_2 fields. We employ improved off-line processing techniques to customize the OMI retrieval for LNO_2. Information on lightning flashes—primarily cloud-to-ground (CG)—observed by the Costa Rica Lightning Detection Network (CRLDN - operated by the Instituto Costarricense de Electricidad) and the World Wide Lightning Location Network (WWLLN) were examined over storms upwind of regions where OMI indicates enhanced LNO_2. These flash data are compared with Tropical Rainfall Measuring Mission/Lightning Imaging Sensor (TRMM/LIS) satellite data to estimate total flashes. Finally, using $[NO_2]/[NO_x]$ ratios from NASA's Global Modeling Initiative model, we estimate LNO_x production per flash for four cases and obtain rates of 100–600 mol/flash. These are near or below rates derived from modeling of observed mid-latitude storms. In our study, environments with stronger anvil-level winds were associated with higher production rates. LIS flash footprint data for one of the low-LNO_x production cases with weak upper tropospheric winds suggest below-average flash lengths for this storm. LNO_x enhancements over background determined from the OMI data were in general agreement with aircraft estimates.

1. Introduction

NO_2 and NO (together referred to as NO_x) are trace gases important in ozone chemistry in both the troposphere and stratosphere. Worldwide, anthropogenic emissions of NO_x dominate the NO_x budget. However, considerable uncertainty surrounds emission rates from natural sources (lightning and soil). Lightning is the largest nonanthropogenic source of NO_x in the free troposphere (hereafter, we refer to lightning-generated NO_x as LNO_x). The most accepted estimates of global LNO_x production range from 2 to 8 Tg (N) yr^{-1} [*Schumann and Huntrieser*, 2007], or about 10–15% of the total NO_x budget. Thunderstorms produce most NO_x in the middle and upper part of the troposphere, where NO_x has a lifetime of 5–10 times longer than the approximate 1-day lifetime in the lower troposphere [*Jaeglé et al*., 1998; *Martin et al*., 2007]. Thus, a given amount of LNO_x in this region can have a greater impact on ozone chemistry than relatively short-lived boundary-layer NO_x. Ozone production can proceed at rates of up to 10 ppbv per day in the lightning-enhanced convective outflow plumes of ozone precursors [*DeCaria et al.,* 2005; *Ott et al.*, 2007; *Pickering et al.,* 1996]. Ozone is the third most important greenhouse gas, and ozone enhancements near the tropopause have the greatest effect on its radiative forcing. Therefore, additional ozone produced downwind of thunderstorm events is particularly effective in climate forcing.

Recent studies have attempted to constrain the magnitude of the global LNO_x source using satellite observations. *Beirle et al*. [2004] used Global Ozone Monitoring Instrument (GOME)

NO_2 column densities over Australia and data from the Lightning Imaging Sensor (LIS) to estimate that lightning produces 2.8 Tg (N) yr^{-1}, but the range of uncertainty was large (0.8–14 Tg (N) yr^{-1}). *Beirle et al*. [2006] studied LNO_x production from a storm system in the Gulf of Mexico using GOME data and National Lightning Detection Network (NLDN) observations. Extrapolating their findings to the global scale, they estimated an LNO_x source of 1.7 Tg (N) yr^{-1} with a range of uncertainty from 0.6 to 4.7 Tg (N) yr^{-1}. *Boersma et al*. [2005] used GOME NO_2 observations and the TM3 global chemical transport model with two different LNO_x parameterizations and concluded that LNO_x production was between 1.1 and 6.4 Tg (N) yr^{-1}. In their study, stratospheric NO_2 was estimated and removed from the data by an assimilation approach using the TM3 model. *Martin et al*. [2007] used Goddard Earth Observing System chemistry model (GEOS-Chem) simulations in conjunction with space-based observations of NO_x, ozone, and nitric acid to estimate LNO_x production of 6 ±2 Tg (N) yr^{-1}. Their NO_2 data were obtained using the Scanning Imaging Absorption Spectrometer for Atmospheric Cartography/chemistry (SCIAMACHY) instrument and analyzed with methods similar to those described in *Martin et al.* [2002]. In general, satellite observations of LNO_x are challenging because of issues of cloud cover and because most upper tropospheric NO_x exists in the form of NO, which is not directly detectable from space. *Beirle et al*. [2009] have demonstrated, through the use of cloud/chemistry and radiative transfer modeling, that nadir-viewing satellites likely have a sensitivity near or less than 50% for LNO_x produced in a typical marine convective system. Therefore, when satellite data are used to estimate LNO_x, this sensitivity factor must be taken into account.

A critical quantity in many studies that attempt to infer global production rates is the rate of NO_x generation in individual thunderstorms, often expressed as the number of moles of NO_x produced per lightning flash. Estimates for this NO_x generation can vary by at least an order of magnitude [*Zhang et al.,* 2003], with many estimates between 50 and 700 mol/flash [*Ott et al*., 2007, 2009 and references therein]. From studies of individual storms, these estimates have been extrapolated to provide global LNO_x production rates. However, such extrapolations are complicated by variations in pressure-level, intensity, and length of lightning strokes for tropical versus mid-latitude storms. The satellite investigation by *Beirle et al*. [2006] found that, on average, lightning in the Gulf of Mexico system produced 90 mol/flash NO. Modeling studies [e.g., *Ott et al.*, 2009] have examined how these parameters vary for intracloud (IC) and cloud-to-ground (CG) flashes in different latitude regions. The variations may result in different LNO_x production rates, P_{IC} and P_{CG}, for IC and CG flashes, respectively. Although early investigations [e.g., *Price et al*., 1997] suggest that the value of the ratio P_{IC}/P_{CG} is much less than 1 (~0.1), more recent studies provide evidence that the value may be near unity or even greater [*DeCaria et al.*, 2005; *Fehr et al.,* 2004; *Ott et al*., 2007, 2009; *Zhang et al.,* 2003]. *Huntrieser et al.* [2008] suggest that overall production of LNO_x per flash, P_{IC+CG}, may be 2–8 times larger in subtropical and mid-latitude storms than in tropical storms. This result may be due to longer flash channel lengths outside the tropics in regions of greater vertical wind shear.

In this paper we examine four tropical convective events from the NASA Tropical Composition, Clouds, and Climate Coupling (TC^4) campaign [*Toon et al*., 2009] and compute the number of moles of LNO_x per flash using a combination of data from the Ozone Monitoring Instrument (OMI) instrument on the Aura satellite, *in situ* observations from the DC-8 aircraft, global chemical transport model output, and ground-based lightning flash observations. Our approach differs from those of previous satellite investigations in the methods used to remove the stratospheric and tropospheric background (as described later in this paper), and because we derive LNO_x production per flash directly from an estimate of accumulated LNO_x and lightning flash counts, rather than by adjusting model parameters to match the satellite data. Our use of OMI data is better suited to individual case studies than are the lower-resolution GOME and SCIAMACHY data. We also focus exclusively on tropical-latitude storms that occurred over ocean regions. In these regions convection is less tied to late-afternoon diurnal cycles (and hence more likely to occur before or near the OMI overpass time of ~13:45 local time [LT]), and NO_2 contamination from anthropogenic sources is less [*Beirle et al.,* 2009]. We use measured OMI NO_2 columns and CG flash counts. From these we estimate the LNO_x columns and the total flashes (IC + CG) and combine results to obtain the P_{CG+IC} for the storms on the 4 days studied. We then examine our results in the context of estimates of LNO_x per flash from other studies.

Section 2 describes the data we used in our analyses. Section 3 details the calculations that were performed in the LNO_x retrieval process and describes how we used the retrieved LNO_x values, in combination with flash rates, to estimate production per flash. Results are presented in Section 4. We discuss the implications of the derived values and their uncertainties in Section 5 and draw conclusions in Section 6.

2. Data Overview

2.1 TC[4]: Aircraft measurements and lightning data

During July and August 2007, NASA launched the TC[4] experiment to study a variety of atmospheric physical and chemical processes in the Eastern Pacific and other areas near Costa Rica. Among TC[4] objectives was validation of measurements from OMI, including cloud properties and column amounts of the trace gases ozone, NO_2, and SO_2. NO and NO_2 measurements at a variety of altitudes near tropical convection were also intended to assess the lightning NO_x budget. In this study, we used *in situ* NO_2 measurements from the University of California at Berkeley's laser-induced fluorescence instrument [*Thornton et al*., 2000, 2003] onboard the NASA DC-8 aircraft, which flew in and around thunderstorms and also sampled relatively undisturbed air in "clean" areas of the Pacific and Caribbean. Figure 1 shows partial DC-8 flight tracks for the sampling within and near convective systems on July 17, 21, and 31, and on August 5.

Observed lightning flashes near the storms of interest were counted so that the per-flash production rates of LNO_x could be determined. In this study, we use flash data from ground-based detectors of the local Costa Rica Lightning Detection Network (CRLDN) and the global scale Worldwide Lightning Location Network (WWLLN) to count flashes from nearby storms on the 4 days examined in this study. The CRLDN records lightning flashes within and near Costa Rica with an efficiency that decreases with distance from the country. The network consists of five IMPACT (Improved Performance from Combined Technology) sensors, similar to those used in the U.S. NLDN [*Cummins et al.*, 1998] distributed throughout Costa Rica. During TC^4, the WWLLN consisted of a network of ~25 detectors distributed throughout the world [*Rodger et al*., 2006]. No complete global observations of the spatial variability of the detection efficiency of WWLLN are available, although the efficiency has been increasing in recent years as the network grows [*Rodger et al*., 2008]. The WWLLN is 30–40% more efficient at detecting flashes with peak currents above 40 kA, which is significantly higher than that of typical CG flashes. There is also some indication that the detection efficiency is greater over ocean than over land in the TC^4 region [*Lay et al*., 2009]. Both detector networks respond primarily to CG flashes and to a smaller percentage of IC flashes. To obtain the total (IC + CG) flash rate, it was necessary to scale the ground-based counts using a reference detector that efficiently recorded both types of flashes. The reference used was data from the LIS instrument on the Tropical Rainfall Measuring Mission (TRMM) [*Boccippio et al.*, 2002] satellite, recorded during all overpasses of Costa Rica and surrounding areas during July and August 2007.

2.2 OMI NO_2 data

The OMI instrument is onboard the Aura satellite, which was launched July 2004 [*Levelt et al*., 2006]. In addition to providing daily global measurements of ozone, OMI records other important trace gases—notably NO_2. Because NO and NO_2 exist in photochemical equilibrium, their sum, NO_x, is the quantity of interest. Due to differences in its absorption spectrum, NO is not readily detectable from space, and the total NO_x amount must be inferred from photochemical models.

The standard NO_2 product from OMI has been described by *Bucsela et al.* [2006, 2008] and *Celarier* [http://toms.gsfc.nasa.gov/omi/no2/OMNO2_readme.pdf]. Backscattered radiation in the form of spectral data from 60 pixels across the satellite track is imaged onto a CCD array, at a spatial resolution of 13×24 km^2 at nadir. The spectrum at each pixel is fitted with an NO_2 absorption cross section to determine the total NO_2 slant column amount, S. In the OMNO2 product, the slant columns are also corrected for an instrumental artifact—the "cross-track anomaly"—with a procedure that cross-track averages data from 15 consecutive orbits between ±55º latitude. The cross-track anomaly correction is computed as an orbital constant at each of the 60 cross-track positions. An air mass factor (AMF), defined as the ratio of a slant column amount to the corresponding vertical column amount, is computed for a stratospheric NO_2 profile and divided into the slant column to give an "initial" vertical column amount. The stratospheric column amount is estimated from the global distribution of initial columns by masking polluted regions and interpolating the remaining field in narrow latitude zones using planetary wave-2 functions. The tropospheric NO_2 vertical column–defined as positive– is computed from the initial and stratospheric amounts and a tropospheric AMF.

For this study, we have developed a different method to estimate tropospheric NO_2 in the regions affected by lightning (items 1 – 6 below). Some of the modifications in our approach (items 1 – 3 and 6) anticipate changes planned for the updated OMI NO_2 standard product data release due in 2009.

(1) Optimize the cross-track anomaly correction for tropical measurements

(2) Apply a correction to the stratospheric field to account for tropospheric contamination

(3) Compute tropospheric NO_2 slant column and allow positive and negative values.

(4) Use observed *in-situ* NO_2 profiles to get AMFs appropriate for convective outflow.

(5) Subtract background (non-lightning NO_2) derived from a global model.

(6) Improve error estimates.

These are discussed further in Section 3.

3. Analysis

In this section we describe our approach for estimating the LNO_x signal from the OMI data. Data from 4 days—July 17, 21, and 31 and August 5, 2007—were selected from the DC-8 flight days during TC^4 for analysis in this study; they are based on the combination of convective activity within 12 hr of OMI overpass, as well as a detectable signal in the OMI NO_2 field near the storms. The lightning signal was too weak to be detectable by OMI in the regions of two additional convective systems sampled by the DC-8 (July 24 and August 8). Some of the analysis also relies on aircraft measurements of *in situ* NO_2 from the DC-8. We also discuss use of the lightning data from ground networks of detectors to obtain total flash estimates for each of the regions studied.

3.1 OMI NO_2 and LNO_x

The LNO_x signal near convection is extracted from the OMI NO_2 data. The procedure involves removal of the stratospheric and background-tropospheric components of the OMI slant columns to yield a lightning-generated NO_2 (LNO_2) slant column. The slant column is divided by an AMF representative of an LNO_x profile to yield the LNO_x vertical column, V_L, which is computed as follows:

$$V_L = [\, S - V_S' \cdot A_S - V_{tBG} \cdot A_{tBG} \,] / A_{tL} \qquad (1)$$

where

- S is the OMNO2 slant column from the spectral fit (corrected for cross-track anomaly)
- V_S' is the corrected stratospheric vertical column amount
- A_S is the AMF for a stratospheric NO_2 vertical profile
- V_{tBG} is the local tropospheric background NO_2 (non-lightning) from the Global Modeling Initiative (GMI) model
- A_{tBG} is the local tropospheric background AMF (to ground) from OMNO2.
- A_{tL} is a factor that converts the LNO_2 slant column to an LNO_x vertical column
- The quantity in brackets in Equation (1)—the LNO_2 slant column—may have positive and negative values.

The slant columns obtained from the OMI spectral fit are corrected for the cross-track anomaly during level-1 to level-2 processing. In this study, we have used a procedure different from that applied in the OMNO2 standard product. Here the data that determine the anomaly are restricted to tropical latitudes between ±30º (rather than the ±55º in OMNO2) and are based on the current orbit, plus 2 adjacent orbits (rather than 15 adjacent orbits). This approach provides sufficient statistics for accurately characterizing the anomaly function, while allowing for variation in the anomaly function during each day and avoiding contamination from polluted regions at middle latitudes.

The second term in Equation (1) is the corrected stratospheric slant column, which appears as the product $V_S' \cdot A_S$, where the stratospheric AMF, A_S, is primarily a function of viewing geometry. The corrected stratospheric field V_S' is given by

$$V_S' = V_S - V_{tc} \cdot \bar{A}_t/\bar{A}_s, \qquad (2)$$

where V_S is the "unpolluted" (essentially stratospheric) field from the wave-2 analysis in the OMNO2 algorithm. This field is based on OMI data from "clean" regions defined by the algorithm's pollution mask. *Martin et al*. [2002] use a related approach in correcting data from the central Pacific. The mask identifies areas that have annual mean tropospheric column amounts less than 0.5×10^{15} cm^{-2}, as estimated from the GEOS-Chem model [*Bey et al*., 2001]. The stratospheric field is constructed from data in these relatively unpolluted areas. However, the small amounts of tropospheric NO_2 in these regions can introduce a significant bias in the V_S, that can mask small amounts of tropospheric NO_2 (e.g., from lightning). We have corrected this in the present study by subtracting zonal mean (within 9º-wide latitude bands) monthly tropospheric column based on the NASA GMI chemical transport model [*Duncan et al*., 2007]. V_{tc} is the mean model tropospheric column in the "clean" regions around the zonal band, and $\bar{A}_t/\bar{A}_s$ is the ratio of the mean tropospheric to stratospheric AMF in the same region. We use a mean value of 0.7 for this ratio. The resulting V_S' is an approximation of the true stratospheric component of the unpolluted field measured by OMI. The difference between V_S and V_S' ranges from 0.04×10^{14} to 0.13×10^{15} cm^{-2} (~2–5%) and has a relatively large uncertainty, as described in Section 5.

The local tropospheric background is the third term in Equation (1). It is a slant column amount equal to the product of the tropospheric vertical column, V_{tBG}, and the tropospheric background AMF, A_{tBG}. Treating the background slant column in this manner neglects potential modification of the background NO_2 profile due to local meteorological effects, but is a good approximation for the small background amounts over tropical oceans [*Beirle et al.*, 2009]. Note, that the AMF, $A_{tBG,}$ is computed from the complete NO_2 profile (tropopause to ground) in the presence of clouds. Thus it implicitly accounts for clouds' effects on the *visibility* of background NO_2 from OMI.

The tropospheric background in the vicinity of the TC^4 study (Central America and surrounding regions) was the monthly mean of GMI model output from a period including late July and early August, averaged over 2005 and 2006 (data from 2007 were not available at the time of this study). The model was run with the NO_x production by lightning turned off, so that only NO_x from non-lightning sources was subtracted from the measurements. The model data are on a 2×2.5^o grid. The GMI model output was used in the background estimation because background values were required for broad regions over and downwind of the convective systems of interest (i.e., over broader regions than the aircraft observed). Other methods of estimating the tropospheric background were examined as discussed in Section 5. The tropospheric AMF was computed using background NO_2 profiles from the GMI model and viewing geometry, and albedo and cloud information from the OMI data product for each measurement (OMI pixel). The background AMF is computed as an integral over pressure, *p*:

$$A_{tBG} = \int \frac{dp}{p} \cdot r_{BG}(p) \cdot a(p) \cdot \beta(p) \qquad (3)$$

where $r_{BG}(p)$ is the background NO_2 mixing-ratio profile, $a(p)$ is the atmospheric scattering weight (a function of viewing geometry, albedo, surface pressure, cloud pressure, and cloud height) and $\beta(p)$ is a temperature correction factor to adjust for the decrease in amplitude of the NO_2 absorption cross section with temperature. Its value for most temperatures in the troposphere and stratosphere is within 20% of unity. Temperatures are climatological monthly means from the National Centers of Environmental Prediction (NCEP). The temperature dependence is approximated as

$$\beta(p) = 1 - 0.003 \cdot [T(p) - 220] \qquad (4)$$

The factor A_{tL} in the denominator of Equation (1), which may be thought of as the "LNO_x AMF", is computed, following *Beirle et al.* [2009], as

$$A_{tL} = \int \frac{dp}{p} \cdot r_{LNO2}(p) \cdot a(p) \cdot \beta(p) \cdot \gamma(p) \qquad (5)$$

In Equation (5), $\gamma(p)$ is the ratio $[NO_2]/[NO_x]$. The ratio depends on local chemistry and photolysis and thus varies with pressure, ozone concentration, and the amount of direct and scattered sunlight available. In this study, three ratios were obtained from the GMI model grid cells in the TC^4 region; they represent maximum, mean, and minimum values for 1800 Universal

Time Coordinated (UTC; near the OMI overpass time) in layers in the typical cloud outflow zone (500 to 100 hPa). The minimum ratio is used for regions above bright clouds, and the mean ratios are used within clouds, down to 100 hPa below cloud tops. The maximum ratios are used in all other regions, including clear areas.

The $\gamma(p)$ profiles are shown along with typical $a(p)$ and $\beta(p)$ profiles in Figure 2. The shapes of the profiles a and β show that radiative transfer effects enhance the sensitivity of the OMI slant column to NO_2 at higher altitudes (above ~600 hPa), where the majority of LNO_2 exists. However, this NO_2 represents only a small fraction of the lightning-generated NO_x, given that the γ profiles have values generally less than 0.5 at these pressure levels.

We used a single composite NO_2 lightning profile, $r_{LNO2}(p)$, in the computation. We assembled it from the four TC^4 DC-8 aircraft profiles containing the highest amounts of NO_2 above the 750 hPa level—the levels most influenced by lightning-generated NO_x. The profiles were binned using median mixing ratios on a fixed pressure grid, similar to the approach used by *Bucsela et al*. [2008]. Because none of the four profiles contained sufficient data above 300 hPa, we used three additional profiles from thunderstorm anvil flights for the composite at these high altitudes. Several of the profiles used for the composite also contained significant amounts of pollution at low altitudes, mostly measured near the airport. Therefore, we extrapolated the mixing ratio of the composite profile at 750 hPa to ground as a constant. The composite LNO_2 profile and a background profile $r_{BG}(p)$ are shown in Figure 2. That profile is qualitatively consistent with the LNO_2 profiles summarized by *Ott et al*. [2009] from the Cirrus Regional Study of Tropical

Anvils and Cirrus Layers-Florida Area Cirrus Experiment (CRYSTAL-FACE), the European Lightning Nitrogen Oxides Project (EULINOX), and the Stratosphere-Troposphere Experiments: Radiation, Aerosols & Ozone (STERAO) campaigns, showing maxima between 4 and 10 km.

The composite profile in this study was used along with OMI pixel information on viewing geometry, albedo, and clouds to construct a value of A_{tL} at each pixel. Since the bulk of LNO_2 is at high altitudes, the value of A_{tL} is relatively independent of the precise shape of the NO_2 profile, particularly in the boundary layer, compared to the AMFs for the background profiles. The primary effect of clouds on A_{tL} is to modify the $[NO_2]/[NO_x]$ ratio. The uncertainty in the final results due to uncertainty in the LNO_2 profile shape (e.g., from constructing the composite without one or more of the individual measured profiles) was found to be negligible relative to other uncertainties in this study, which are discussed in Section 5.

A perimeter, constructed on a 1º-longitude x 1º-latitude grid defines the estimated region influenced by lightning NO_x for the day in question. The regions were selected on the basis of the location of recent (within the past 12 hr) convection, the mean upper-tropospheric wind fields, and examination of the OMI NO_2 field. The regions were designed to minimize potential effects by other convective systems. However, such effects remain a possible source of contamination and represent a significant uncertainty in each of the case studies, except the July 17 case.

The value of V_L was obtained from Equation (1) for pixels having centers within the perimeter, and a weighted sum was computed. Weights were based on the approximate area of overlap for the pixel with the region. The total number of moles LNO_2 in region is the average V_L, times the area of the region, divided by Avagadro's number.

3.2 Flash counts

The CRLDN and concurrent LIS data were binned in concentric rings in radius steps of 200 km around the middle of Costa Rica. The data were obtained from all LIS overpasses over or near Costa Rica during July and August 2007. Only CRLDN flashes that occurred within the LIS field of view were considered in this analysis. From these data, we derived detection fractions for total flashes (CG + IC) in each ring. The scaling factor for CRLDN data, ε_C (the inverse of detection fraction) is:

$$\varepsilon_C = \langle F_{LIS} / F_{CRLDN} \rangle \qquad (6)$$

where F_{LIS} are the LIS satellite flash counts, F_{CRLDN} are the raw CRLDN counts, and $\langle\ \rangle$ refers to averaging in a given ring over the 2 months. Before their use in this calculation, we adjusted the LIS flash counts for the detection efficiency of this instrument on the basis of values provided by *Boccippio et al*. [2002] (e.g., 69% at local noon and 88% at night). Values of ε_C determined for this period were 1.40 in the 0–200 km radius ring, 2.80 in the 200–400 km radius ring, and 9.17 in the 400–600 km ring. Beyond 600 km, the CRLDN data become too uncertain to use in LNO_x analyses. We used ε_C to obtain adjusted CRLDN counts, F'_{CRLDN}, for the July 31 storm, which was located near the CRLDN network, and took this value to be the best estimate of total number of flashes for that storm; that is,

$$F_{Total} = F'_{CRLDN} = F_{CRLDN} \cdot \varepsilon_C \qquad (7)$$

We also estimated the detection fraction of the WWLLN network in the TC^4 region. The flash counts from the CRLDN (adjusted using ε_C) and WWLLN for six storms during the TC^4 period in the vicinity of Costa Rica were compared to obtain a second scaling factor ε_W. The factor is

$$\varepsilon_W = \langle F'_{CRLDN} / F_{WWLLN} \rangle \qquad (8)$$

where F_{WWLLN} is the WWLLN flash count. In this case, no information on the spatial variability of the WWLLN is available, because the averaging was done over six storms, all of which were near Costa Rica. We obtained a mean value $\varepsilon_W = 4.57$ with an error of ±36%. This factor was used to compute the total flash counts on July 17 and 21 and August 5, when storms were relatively far from the CRLDN network; that is,

$$F_{Total} = F_{WWLLN} \cdot \varepsilon_W \qquad (9)$$

Dividing the estimated total flash counts into the moles of LNO_x in the corresponding region gives the estimated number of mole per flash.

4. Results

We obtained measurable OMI NO_2 signals near convection on 4 of the 6 days during the TC^4 experiment on which the aircraft sampled thunderstorm anvils. All four convective systems analyzed are located over the ocean. Therefore, convective transport of surface emissions of NO_x

into the anvils of these systems was assumed to be negligible. By comparing the OMI NO_2 field with the cloud field and lightning measurements, and estimating the effects of transport due to mid-tropospheric wind fields, we identified regions of possible LNO_x enhancement. The OMI effective geometrical cloud fraction on those days is shown in Figure 3, and the LNO_x fields over the same areas, computed as outlined in Section 3, are shown in Figure 4.

Most of the regions in Figure 3 are partly cloudy, and we estimate values of A_{tL}, between 0.2 and 0.8, with most values in the range of 0.4 to 0.5. These factors compare well with the factors estimated in the model study of *Beirle et al* [2009] (referred to as "sensitivity factors" in that study), in spite of the simpler fixed LNO_2 profile and approximation of opaque Lambertian clouds used in the present study. *Ott et al*. [2009] estimated the LNO_2 signal that might be seen in satellite measurements over convective clouds, based on visible-near-UV penetration of radiation to a depth of 400–600 hPa. Their calculations suggested LNO_2 tropospheric vertical columns of $0.1 – 2.0 \times 10^{15}$ cm^{-2} should be detectable over active convection. In the present study, the mean LNO_2 column in each of the regions analyzed ranged from $0.2 – 1.7 \times 10^{15}$ cm^{-2}.

Table 1 summarizes information about the regions studied on the 4 days. Shown are the areas of the polygons, the mean anvil-level wind velocities from NCEP reanalysis, the moles of LNO_x, flash counts, and the resultant LNO_x production rates. Derivation of the uncertainty estimates is given in Section 5.

LNO_x production per flash was found to be relatively low—between 100 and 200 mol/flash—in the first two cases (July 17 and 21) and higher—400 to 600 mol/flash—in the latter two cases (July 31 and August 5). We note that the first two cases had relatively light anvil-level (300 hPa) wind speeds (2–6 m/s) and that the latter two cases had stronger winds at anvil level (8–13 m/s). These results are suggestive of agreement with the results of *Huntrieser et al*. [2008], who found greater LNO_x production in storms with greater vertical wind shear. The *Huntrieser et al*. analysis suggests that longer flash length occurs with stronger upper level winds and that the greater length is responsible for greater production per flash. *Huntrieser et al*. [2009] suggest that even within the tropics substantial variability in production per flash can occur, and may also be related to flash length and associated wind profiles.

5. Discussion

The moles per flash estimates in this study are associated with large uncertainties. In this section we examine the error estimates and compare our results with those of other studies.

5.1 Uncertainties

The small magnitude and spatial extent of LNO_2 enhancements make precise measurements difficult, as reflected in the large uncertainties in moles per flash obtained this study. We distinguish between two types of errors: (1) those related to pixel-scale measurement variability, which we treat as random errors, and (2) systematic errors associated with larger scale variability. The latter are the largest component of the overall uncertainties in the moles per flash numbers. In this section we discuss the estimation of both types of errors and their propagation. To identify all sources of uncertainty, Equation (1) can be rewritten explicitly as follows:

$$V_L = \sum_i w_i \cdot \{ S_i - [V_{si} + \delta V_s - (V_{tc\,i} + \delta V_t) \cdot \bar{A}_t/\bar{A}_s] \cdot A_{si} - (V_{tbg\,i} + \delta V_t) \cdot A_{tbg\,i} \} / A_{tLi} \quad (10)$$

The summation in Equation (10) is over all pixels, i, in the region of interest (bounded by the perimeters in Figures 3). The individual pixel errors are computed independently for each term subscripted with i and are assumed, for simplicity, to be uncorrelated. Here w_i is the weighting factors based on the pixel area. The errors in the slant columns, S_i, were derived in the spectral fit and found to be consistent with the pixel-to-pixel spatial variability of slant columns. The terms δV_s and δV_t are modifications to Equation (1) and identify sources of systematic error, relatively independent of individual pixels. They stand for potential biases in the derived OMNO2 stratosphere and the GMI model troposphere, respectively. These terms, described below, have mean values of zero, but are given fixed finite uncertainties, independent of pixel area.

Random errors at each pixel make a relatively small contribution to the total error budget. The random uncertainty in the OMI stratospheric column, V_{si}, is conservatively estimated to be 0.2×10^{15} cm^{-2} [*Boersma et al.*, 2004; *Bucsela et al.,* 2006]. The model column amount $V_{tc\,i}$ is assigned a random error of 40%, based on a set of clean profiles measured during TC^4 and consistent with GMI model variability in the region of the TC^4 study (see Figure 5). The same 40% random error is assumed for $V_{tbg\,i}$, also from GMI. Errors in the AMFs depend on estimates of cloud parameters, surface albedos, and a priori profile shape variability. They are computed using an off-line algorithm [*Wenig et al*., 2008] that improves on the OMNO2 collection 3 uncertainties. Of the error sources contributing the AMF uncertainty, the largest are associated with clouds, which can shield or enhance the visibility of NO_2 and affect the NO_x photolysis ratio. Uncertainty in the latter was not explicitly considered in this study.

The uncertainty in δV_s is based on an estimate of the potential error introduced by the wave-2 method used to derive the stratosphere in the OMI NO_2 algorithm. Other NO_2 satellite retrieval algorithms employ the Pacific Reference Sector (PRS) method [e.g., *Martin et al.*, 2002; *Richter and Burrows*, 2002], which assumes a constant stratospheric amount at each latitude based on data over the central Pacific Ocean at that latitude. The DOMINO algorithm used to process OMI NO_2 data for the Dutch near-real time product assimilates OMI slant columns into the TM4 model, weighting the data according to model estimates of tropospheric contamination [*Boersma et al.*, 2007]. Our comparisons of these models show that stratospheric estimates at middle and high latitudes can differ by as much as 0.5 to 1.0×10^{15} cm^{-2}. At tropical latitudes, the differences tend to be smaller—on the order of 0.1 to 0.2×10^{15} cm^{-2}. Stratospheric fields from both methods for the July 21 case are shown in Figure 5. For the 4 days examined in this study, the PRS and wave-2 methods were tested and gave mean stratospheric values that varied by 0.01 to 0.11×10^{15} cm^{-2}, with an average difference of 0.07×10^{15} cm^{-2}. Both methods of stratospheric field estimation can also be affected by the decision to cloud-screen the pixels used to construct the field. We found that using only pixels from relatively clear skies (cloud radiance fractions less than 50%) changed the resultant mean stratospheric value in the TC^4 region by $\sim 0.04 \times 10^{15}$ cm^{-2}. Combining the uncertainties introduced by cloud screening with those associated with the PRS vs. wave-2 methods gave a potential systematic uncertainty of about 0.1 $\times 10^{15}$ cm^{-2} (or about 4%) in the tropical stratosphere.

The systematic error in δV_t, representing a potential bias in the GMI troposphere over “clean” regions, is hard to estimate. One approach is to use an alternative analysis based on a uniform measured background, rather than the GMI no-lightning model values. To test this, we computed a value for A_{tBG} by integrating a fixed composite profile, made up of a group of DC-8 measured profiles that showed relatively small amounts of NO_2 in the region above 600 hPa, where most LNO_2 is typically found. The vertical column obtained by integrating this profile from ground to GMI-estimated tropopause pressure of 100 hPa is approximately 0.67 cm^{-2} ±0.29. This value is considerably larger than the GMI background values for tropospheric NO_2, which ranged from 0.2 to 0.5 $\times 10^{15}$ cm^{-2}. The results of the fixed-background analysis yielded LNO_x values that were less than zero in approximately 40% of the cases around the anvil and outflow regions, indicating the uniform background to be an overestimate. Such a background is also inconsistent with the GMI model, which indicates a variable background that decreases from north to south across the region. Although the measured profiles used for the composite were selected from the DC-8 profiles with the lowest mixing ratios, it is still possible that they contained some LNO_2 contamination. Because the experimental region experienced lightning every day, it was difficult to find any air masses that were totally devoid of LNO_2 influence. Most of the background profiles showed some increase in NO_2 with altitude in the upper troposphere, indicative of a lightning contribution. Moreover, the mixing ratios in these measured profiles are near the detection limit of the LIF instrument on the DC-8. For this reason, we have adopted the GMI model output to represent the background NO_2 and have assigned these background vertical columns a nominal systematic uncertainty of $\delta V_t = 0.15 \times 10^{15}$ cm^{-2}, which is on the same order as the spatial variability of the GMI model background. Note that the precise value of this systematic uncertainty is less critical than is the uncertainty in δV_s because the two terms in Equation (4) containing δV_t partially cancel each other. Figure 6 shows the GMI no-lightning background tropospheric columns based on a 2-year mean for July and August.

A large source of error in the computed moles of LNO_x results from the selection of the geographic area of interest. One component is imprecise knowledge of the wind fields, which makes the position of the regions' centers uncertain. We did not attempt detailed trajectory analysis of the convective outflow in this study, given the difficulty in estimating convective perturbations to the analyzed ambient winds during the few hours between storm development and OMI overpass. Therefore, we have used the mean wind speed and direction in the vicinity of the storm and immediately downwind from the 300 hPa NCEP analysis and the number of hours between storm development and the OMI overpass to estimate the region affected by the outflow. This region generally corresponded to the location of enhancements in LNO_x downwind of the storm. Assuming the 10–15% variability of the analyzed winds from NCEP and lightning occurring throughout a 12-hr period preceding the OMI overpass, we estimate the transport distance along the mean wind vectors to have an error less than or equal to ±0.3° of latitude. Adjusting the geographic positions of the regions by this amount along the wind vectors allows us to estimate the sensitivity of the LNO_x calculation to the wind field.

Another uncertainty in the region selection is the size of each area. We estimate that storm-outflow regions can be identified in the OMI NO_2 field to a resolution of approximately 1º and have drawn the perimeters in each case accordingly (see Figure 4). From this we obtain the approximate uncertainty in the enclosed areas following the approach of *Ghilani* [2000] and uniformly expand and shrink the regions by the same amount to determine the effect on the derived moles of LNO_x.

The combined effects of the uncertainties in the regions' areas and positions lead to uncertainties in the computed number of moles on the order of 15–35%. The areal uncertainty makes the largest contribution. Further uncertainties exist because of the possible contamination due to LNO_x from neighboring convective systems, for which lightning counts were not available. Although the region perimeters were drawn to minimize such contamination, nearby storms potentially influenced the results for each day, except July 17. Because we did not estimate the magnitude of this influence in this study, the moles LNO_x and moles per flash estimates we obtained must be considered upper limits, and the uncertainties may be larger than those indicated here.

The final source of error is uncertainty in the number of flashes that contribute to the LNO_x enhancements. The flash-count error depends on the method used to obtain the counts. For the July 31 case, the adjusted counts were obtained from the CRLDN and have an error of 10–20%. In the other cases, the adjustment factor $\varepsilon_W = 4.57$ used to scale the WWLLN has an uncertainty of ±1.66, or 36%.

Table 2a summarizes the error sources in the calculation of LNO_x, and Table 2b shows their contributions along with those of flash uncertainties to the overall error in each of the four cases. The largest sources of error are the systematic error in the stratosphere and tropospheric background over the region, as well as the region-selection error. The uncertainty in the flash count rate makes a smaller contribution. The random variations can be large for a given pixel, but are a small part of the error budget due to the statistical averaging of a large number of OMI pixels. Although our calculation of the relative error is largest for the July 17 case, this case was less affected by neighboring convection (which is not explicitly accounted for here) than by the other days; consequently, the actual uncertainties on those days may be larger than shown.

5.2 LNO_x from OMI in compared with TC^4 aircraft data

Here we compare the NO_x enhancement over background due to lightning as computed from OMI with that estimated from the *in situ* DC-8 observations within and near the observed convective systems. For times when either NO or NO_2 was missing from the aircraft data set, we estimated it using a photostationary state calculation. Table 3 presents the means and standard deviations of the in-cloud and nearby clear-air aircraft observations, the OMI LNO_x column amounts, and the column amounts of NO_x in the tropospheric background as estimated by the no-lightning GMI model. The aircraft enhancements are computed as the ratio of the in-cloud measurements to the clear-air measurements. The LNO_x enhancement in the broader-scale convective outflow (as seen by OMI) should be roughly proportional to the in-anvil enhancement (as measured by the DC-8). The DC-8 data show enhancement factors due to lightning of between 1.74 and 2.35. Enhancements in the OMI LNO_x column are calculated as the sum of OMI + background, divided by background. The OMI enhancement factors are in the range of 1.43 to 2.14, and show day-to-day variations consistent with those of the DC-8 factors. Therefore, the DC-8 observations verify the OMI-based LNO_x enhancement.

5.3 Other studies of LNO_x production per flash

The production efficiencies for LNO_x from the storms in this study range from <200 to ~600 mol/flash. The wide range is not surprising, given the range found in the literature and the large uncertainties in the results. However, the mean value over the 4 cases of 368 mol/flash compares well with the 360 mol/flash obtained by *Ott et al*. [2007] in their analysis of a mid-latitude storm. The two lower values obtained in this study (for July 17 and 21) are comparable to the production efficiencies obtained in tropical and subtropical storms by *Huntreiser et al.* [2008] during the Brazilian Tropical Convection, Cirrus and Nitrogen Oxides Experiment (TROCCINOX) experiment. Using total flash counts derived from LIS measurements, *Huntreiser et al.* [2008] estimated production of 1–3 kg(N)/flash, which corresponds to ~70–200 mol/flash. They hypothesized that the smaller production rates for the lower latitude storms were related to disparities in production by flashes at different latitudes, as we discuss below.

Ott et al. [2009] summarized analyses of five mid-latitude and subtropical storms simulated using a 3-D cloud-scale model. The storms were observed during the STERAO, EULINOX, and CRYSTAL-FACE field campaigns. They derived production efficiencies for CG flashes, based on observations of the CG and IC flash rates and on comparisons of their model simulations with aircraft observations of NO_x in the storms. They also compared their results to estimates of P_{CG} from *Price et al*. [1997] and *Fehr et al*. [2004]. With the exception of the *Price et al*.'s [1997] theoretical value of $P_{IC}/P_{CG} = 0.1$, most recent results indicate that IC and CG flashes produce equal amounts of NO on average, in agreement with the recommendation of *Ridley et al*. [2005]. Therefore, for the purpose of comparing results of the present study with the P_{CG} and P_{IC} estimates from *Ott et al*. [2009] and other studies, we adopt a value of unity for P_{IC}/P_{CG}. These comparisons are shown in Figure 7 as a function of latitude and anvil-level wind speed. Although there appears to be no universal relationship linking production per flash to latitude or anvil-level wind speed, within regions or within particular experiments the larger production per flash values are associated with the stronger upper-level winds.

The average number of moles per flash over the four cases from the present study of tropical convection (~350) is lower than the ~500 mol/flash average derived from the mid-latitude and subtropical storms of the *Ott et al*. [2009] study. *Ott et al*. extrapolated the 500 mol/flash to estimate global LNO_x production at 8.6 Tg (N) yr^{-1}, which is near the high end of the range of 2 to 8 Tg (N) yr^{-1} from *Schumann and Huntrieser* [2007]. They suggest the high value may be due to neglect of tropical storms in their study. The lower production rates of the present TC^4 study are consistent with the hypothesis that tropical storms produce, on average, less NO_x per flash than do storms at higher latitudes. A possible mechanism is that flashes in tropical thunderstorms are less productive than flashes in mid-latitude storms. In general, the LNO_x production rate for a given flash depends on the intensity of the flash, the flash length, and the pressures at which the flash occurs. Although a greater fraction of a CG flash occurs at higher pressure than an IC, this effect may be counterbalanced, in mid-latitude storms by the longer IC flash lengths (*Ott et al*., 2007; 2009), leading to near equal LNO_x production per flash for IC and CG flashes. *Huntrieser et al*. [2008] hypothesize that flash lengths in mid-latitudes and subtropics are greater than flash lengths in the tropics because of greater vertical wind shear at the higher latitudes—leading to greater LNO_x production per flash outside of the tropics. The storms of July 17 and 21 had production efficiencies (averaged over IC and CG flashes) consistent with the tropical and subtropical TROCCINOX analysis of *Huntreiser et al*. [2008], but for the storms of July 31 and August 5 we have derived larger values. Anvil-level winds were stronger in the 300 hPa NCEP reanalysis fields for July 31 and August 5 than for July 17 and 21, suggesting possible longer flash lengths in these cases, with greater LNO_x production per flash. It is also possible that contamination from nearby convection (not included in the flash counts) may have contributed to the larger LNO_x amounts on those days, but this may have also been the case for one of the days with low LNO_x production rate (July 21).

5.4 Flash footprints

Further evidence for the effects of wind shear may be seen in the LIS data, which can be used to obtain information on the extent of lightning flashes. The LIS sensor operates as a lightning event detector on a charge coupled device (CCD). An event is defined as the occurrence of a single CCD pixel exceeding the background threshold during a single frame. Because a single pixel will almost never correspond to the exact cloud illumination area, a lightning discharge will often illuminate more than one pixel during a single integration time. The result is two or more events that are clustered in space and time (groups). A lightning flash may also correspond to several related groups in a limited area [*Christian et al*., 1994]. Integrating the area of all CCD pixels involved in a flash provides the "footprint" of the flash [*Boccippio* et al., 1998], which can be interpreted as its horizontal extent.

LIS viewed only one of the four storms analyzed here (July 21). Figures 8a and 8b show, respectively, the flash rate density and the event rate density of the July 21 case. It can be seen that all convective cores of the cloud (orange tones in Figure 1b) produced flashes, at a rate up to 7.46 flashes km^{-2} s^{-1} on the north cell. Although only a few flashes were detected in the center of the storm, the event rate density shows that area illuminated by those flashes corresponds to a fairly large extent of the convective cores, delineating the sum of flash footprints. The statistics of individual flash footprints of the July 21 case is presented in Figure 8c, and is compared to the statistics of all LIS flashes recorded throughout the tropics (35^{o}S to 35^{o}N) during the boreal summer (June, July and August) of 2007 (Figure 8d). Note that the distribution for the July 21 storm north of Colombia is skewed toward smaller footprint sizes (<556 km^2) compared with the nearly perfect Gaussian distribution for 2007 boreal summer. Assuming that the LIS footprint can be considered a proxy for flash length, this result suggests that there was a greater frequency of short flashes for this storm than is typical for this latitude band. The small magnitude of the LNO_x production per flash obtained from our analysis of OMI NO_2 data for this storm, combined with the weak upper tropospheric wind speeds and the smaller LIS footprint, supports the *Huntrieser et al*. [2008] hypothesis.

6. Conclusions

We have developed an algorithm to retrieve realistic LNO_x signals from OMI. Improvements over the standard retrieval include a more exact treatment of the stratospheric NO_2 column and an improved cross-track anomaly correction. To customize the retrieval for LNO_x, we have removed background tropospheric NO_2 column amounts using the GMI model, and used an AMF appropriate for a profile shape characteristic of convective outflow (based on TC^4 aircraft observations). The technique has been applied to four TC^4 flight day convective events occurring over the ocean offshore from Costa Rica, Panama, and Colombia. Combining these TC^4 data with flash observations, we estimate LNO_x production per flash for each of the selected cases. Preliminary results show that LNO_x production per flash was in the 400–600 mol range for two cases with stronger upper level winds, and 100–200 mol for two cases with weaker anvil-level transport, suggesting that tropical LNO_x values can be at or below those found at higher latitudes. Flash footprint size information from the LIS instrument suggests that for the storm with the smallest LNO_x production per flash estimate the flash lengths were shorter than is typical. The enhancement due to LNO_x above background levels determined using OMI NO_2 data is in agreement with the enhancement seen in *in situ* anvil NO_x observations over background observations taken by the DC-8 aircraft in TC^4, thereby providing validation of the LNO_x retrieval method.

Acknowledgements

This research was supported by the NASA Aura Validation Program. Lightning data from the Costa Rica Lightning Detection Network were provided by Instituto Costarricense de Electricidad.

References

Beirle, S., N. Spichtinger, A. Stohl, K. L. Cummins, T. Turner, D. Boccippio, O. R. Cooper, M. Wenig, M. Grzegorski, U. Platt, and T. Wagner, (2006), Estimating the NO_x produced by lightning from GOME and NLDN data: A case study in the Gulf of Mexico, *Atmos. Chem. Phys.*, *6*, 1075–1089.

Beirle, S., U. Platt, M. Wenig, and T. Wagner, (2004), NO_x production by lightning estimated with GOME, *Adv. Space Res.*, *34*(4), 793–797.

Beirle, S., M. Salzmann, M. G. Lawrence, and T. Wagner, (2009), Sensitivity of satellite observations for freshly produced lightning NO_x, *Atmos. Phys. Chem.*, *9*, 1077–1094.

Bey, I., D. J. Jacob, R. M. Yantosca, J. A. Logan, B. D. Field, A. M. Fiore, Q. Li, H. Y. Liu, L. J. Mickley, and M. G. Schultz, (2001), Global modeling of tropospheric chemistry with assimilated meteorology: Model description and evaluation, *J. Geophys. Res.*, *106*, 23073–23096.

Boccippio, D. J., W. J. Koshak, and R. J. Blakeslee, (2002), Performance assessment of the Optical Transient Detector and Lightning Imaging Sensor. Part I: Predicted diurnal variability, *J. Atmos.Oceanic Technol.*, *19*, 1318–1332.

Boccippio, D., K. Driscoll, J. Hall, and D. Buechler (1998), LIS/OTD Software Guide, Global Hydrology and Climate Center, pp.142. Available on-line at ftp://ghrc.nsstc.nasa.gov/pub/doc/lis/LISOTD_UserGuide.pdf

Boersma, K. F., H. J. Eskes, and E. J. Brinksma, (2004), Error analysis for tropospheric NO_2 from space, *J. Geophys. Res., 109*, D04311, doi:10.1029/2003JD003962.

Boersma, K. F., H. J. Eskes, E. W. Meijer, and H. M. Kelder, (2005), Estimates of lightning NO_x production from GOME satellite observations, *Atmos. Chem. Phys., 5*, 2311–2331.

Boersma, K. F., H. J. Eskes, J. P. Veefkind, E. J. Brinksma, R. J. van der A, M. Sneep, G.H.J. van den Oord, P. F. Levelt, P. Stammes, J. F. Gleason, and E. J. Bucsela, (2007), Near-real time retrieval of tropospheric NO_2 from OMI, *Atmos. Chem. Phys., 7*, 2103–2118.

Bucsela E., E. Celarier, M. Wenig, J. F. Gleason, P. Veefkind, K. F. Boersma, and E. Brinksma, (2006), Algorithm for NO_2 vertical column retrieval from the Ozone Monitoring Instrument, *IEEE Trans. Geosci. Remote Sensing, 44,* 1245–1258.

Bucsela, E. J., A. E. Perring, R. C. Cohen, K. F. Boersma, E. A. Celarier, J. F. Gleason, M. O. Wenig, T. H. Bertram, P. J. Wooldridge, R. Dirksen, and J. P. Veefkind, (2008), Comparison of tropospheric NO_2 from in situ aircraft measurements with near-real-time and standard product data from OMI, *J. Geophys. Res*., *113*, D16S31, doi:10.1029/2007JD008838.

Christian, H., R. Blakeslee, S. Goodman, and Douglas Mach (1994), Algorithm Theoretical Basis Document (ATDB) for the Lightning Imaging Sensor (LIS), George C. Marshall Space Flight Center, National Aeronautics and Space Administration. Available on-line at http://eospso.gsfc.nasa.gov/eos_homepage/for_scientists/atbd/docs/LIS/atbd-lis-01.pdf

Cummins, K. L., M. J. Murphy, E. A. Bardo, W. L. Hiscox, R. B. Pyle, and A. E. Pifer, (1998), A combined TOA/MDF technology upgrade of the U.S. National Lightning Detection Network, *J. Geophys. Res., 103*, 9035–9044.

DeCaria, A. J., K. E. Pickering, G. L. Stenchikov, and L. E. Ott, (2005), Lightning-generated NO_x and its impact on tropospheric ozone production: A three-dimensional modeling study of a Stratosphere-Troposphere Experiment: Radiation, Aerosols and Ozone (STERAO-A) thunderstorm, *J. Geophys. Res*, *110*, D14303, doi:10.1029/2004JD005556.

Duncan, B. N., S. E. Strahan, Y. Yoshida, S. D. Steenrod, and N. Livesey, (2007), Model study of the cross-tropopause transport of biomass burning pollution, *Atmos. Chem. Phys.*, *7*, 3713–3736.

Fehr, T., H. Höller, and H. Huntrieser, (2004), Model study on production and transport of lightning-produced NO_x in a EULINOX supercell storm, *J. Geophys. Res.*, *109*, D09102, doi:10.1029/2003JD003935.

Ghilani, C. D., (2000), Demystifying area uncertainty: More or less. *Survey. Land Inf. Syst.,* *60*(3):177–182.

Huntrieser, H., U. Schumann, H. Schlager, H. Holler, A. Giez, H.-D. Betz, D. Brunner, C. Forster, O. Pinto Jr, and R. Calheiros, (2008), Lightning activity in Brazilian thunderstorms during TROCCINOX: Implications for NO_x production, *Atmos. Chem. Phys*., *8*, 921–953.

Huntrieser, H., H. Schlager, M. Lichtenstern, A. Roiger, P. Stock, A. Minikin, H. Hoeller, K. Schmidt, H.-D. Betz, G. Allen, S. Viciani, A. Ulanovsky, F. Ravegnani, and D. Brunner, (2009), NO_x production by lightning in Hector: First airborne measurements during SCOUT-O3/ACTIVE, *Atmos. Chem. Phys. Discuss.*, *9*, 14361–14451.

Jaeglé, L., D. J. Jacob, Y. Wang, A. J. Weinheimer, B. A. Ridley, T. L. Campos, G. W. Sachse, and D. E. Hagen, (1998), Sources and chemistry of NO in the upper troposphere over the United States, *Geophys. Res. Lett.*, *25*, 1709–1712.

Lay, E. H., C. J. Rodger, R. H. Holzworth, A. R. Jacobson, D. M. Suszcynsky, J. N. Thomas, and J. B. Brundell, (2009), World-wide Lightning Location Network: Improvements in global detection efficiency and estimated stroke energy, Fourth Conference on the Meteorological Applications of Lightning Data, American Meteorological Society, Phoenix, AZ.

Levelt, P. F., E. Hilsenrath, G. W. Leppelmeier. G.B.J. van den Oord, P. K. Bhartia, J. Tamminen, J. F. de Haan, and J. P. Veefkind, (2006) Science objectives of the Ozone Monitoring Instrument, *IEEE Trans. Geosci. Remote Sensing, 44*, 1199–1208.

Martin, R. V., K. Chance, D. J. Jacob, T. P. Kurosu, R. J. D. Spurr, E. Bucsela, J. F. Gleason, P. I. Palmer, I. Bey, A. M. Fiore, Q. Li, R. M. Yantosca, and R.B.A. Koelemeijer, (2002), An improved retrieval of tropospheric nitrogen dioxide from GOME, *J. Geophys. Res.*, *107*(D20), art. no. 4437.

Martin, R. V., B. Sauvage, I. Folkins, C. E. Sioris, C. Boone, P. Bernath, and J. Ziemke, (2007), Space-based constraints on the production of nitric oxide by lightning, *J. Geophys. Res.*, *112*, D09309, doi:10.1029/2006JD007831.

Ott L. E., K. E. Pickering, G. L. Stenchikov, H. Huntrieser, and U. Schumann, (2007), Effects of lightning NO_x production during the 21 July European Lightning Nitrogen Oxides Project storm studied with a three-dimensional cloud-scale chemical transport model, *J. Geophys. Res.*, *112*, D05307, doi:10.1029/2006JD007365.

Ott, L. E., et al., (submitted, 2009), Production of lightning NO_x and its vertical distribution calculated from 3-D cloud-scale chemical transport model simulations, *J. Geophys. Res*.

Pickering, K., et al., (1996), Convective transport of biomass burning emissions over Brazil during TRACE A, *J. Geophys. Res.*, *101*(D19), 23993–24012.

Price, C., J. Penner, and M. Prather, (1997), NOx from lightning, 1. Global distributions based on lightning physics, *J. Geophys. Res*., *102*, 5929–5941.

Richter, A., and J. P. Burrows, (2002), Tropospheric NO_2 from GOME measurements, *Adv. Space Res*., *29*, 1673.

Ridley, B., K. Pickering, and J. Dye, (2005), Comments on the parameterization of lightning-produced NO in global chemistry-transport models, *Atmos. Environ.*, *39*, 6184–6187.

Rodger C. J., S. W. Werner, J. B. Brundell, N. R.Thomson, E. H. Lay, R. H. Holzworth, and R. L. Dowden, (2006), Detection efficiency of the VLF World-Wide Lightning Location Network (WWLLN): Initial case study, *Ann. Geophys*., *24*, 3197–3214.

Rodger, C. J., J. B. Brundell, R. H. Holzworth, and E. H. Lay (2009), Growing Detection Efficiency of the World Wide Lightning Location Network, *Am. Inst. Phys. Conf. Proc*., Coupling of thunderstorms and lightning discharges to near-Earth space: Proceedings of the Workshop, Corte (France), 23-27 June 2008, 1118, 15-20, DOI:10.1063/1.3137706. http://wwlln.net/publications/rodger_WWLLN_TLE_final_23Jan09.pdf

Schumann, U., and H. Huntrieser, (2007), The global lightning-induced nitrogen oxides source, *Atmos. Chem. Phys*., *7*, 3823-3907.

Thornton, J. A., P. J. Wooldridge, and R. C. Cohen, (2000), Atmospheric NO_2: *In situ* laser-induced fluorescence detection at parts per trillion mixing ratios, *Anal. Chem.*, *72*, 528–539.

Thornton, J. A., P. J. Wooldridge, R. C. Cohen, E. J. Williams, D. Hereid, F. C. Fehsenfeld, J. Stutz, and B. Alicke, (2003), Comparisons of *in situ* and long path measurements of NO in urban plumes, *J. Geophys. Res*., *108*, (D16), 4496, doi:10.1029/2003JD003559.

Toon, O. B., et al., (submitted, 2009), Planning and implementation of the Tropical Composition, Clouds and Climate Coupling Experiment (TC^4), *J. Geophys. Res*.

Wenig, M. O., A. M. Cede, E. J. Bucsela, E. A. Celarier, K. F. Boersma, J. P. Veefkind, E. J. Brinksma, J. F. Gleason, and J. R. Herman, (2008), Validation of OMI tropospheric NO_2 column densities using direct-sun mode Brewer measurements at NASA Goddard Space Flight Center, *J. Geophys. Res*., *113*, D16S45, doi:10.1029/2007JD008988.

Zhang X., J. H. Helsdon Jr., and R. D. Farley, (2003), Numerical modeling of lightning-produced NO_x using an explicit lightning scheme: 2. Three-dimensional simulation and expanded chemistry, *J. Geophys. Res*., *108*(D18), 4580, doi:10.1029/2002JD003224.

Figure Captions

Figure 1: Partial DC-8 flight tracks in the vicinities of storms sampled on (a) July 17, (b) July 21, (c) July 31, and (d) August 5, 2007 during the TC^4 mission superimposed on Geostationary Operational Environmental Satellite (GOES-10/12) color-enhanced infrared images. Insets show the pressure altitude during flight.

Figure 2: Profiles involved in AMF calculations in this study, (a) r_{BG} = background NO_2, r_{LNO2}= lightning NO_2, (b) a = atmospheric scattering weight, β = temperature correction factor, γ = three profiles representing the $[NO_2]/[NO_x]$ ratio. The profiles r_{LNO2} and r_{BG} are fixed. All others depend on pixel location (typical examples are shown here).

Figure 3: OMI effective geometrical cloud fraction (at the time of OMI overpass) on the four dates in this study (a) July 17, (b) July 21, (c) July 31, and (d) August 5, 2007. The polygons outline regions examined for enhanced NO_2 due to lightning.

Figure 4: Vertical column densities of LNO_x inferred from OMI data, for (a) July 17, (b) July 21, (c) July 31, and (d) August 5, 2007. The polygons outline regions examined for enhanced NO_2 due to lightning.

Figure 5: Corrected stratospheric field, estimated from OMI data for July 21, 2007 (a) using the planetary-wave analysis up to wave-2, and (b) using the PRS method. Both fields have been

corrected by subtracting a model GMI tropospheric background, equal to approximately 5% of the stratospheric column value.

Figure 6: Tropospheric background computed from the GMI model (with the lightning source turned off) for July and August. Asterisks mark the locations of DC-8 NO_2 profile measurements, taken over several TC^4 days, and used to construct the background profile that we compare with the GMI model (see text).

Figure 7: Mean LNO_x production, P_{IC+CG}, for all lightning flashes produced by storms analyzed in TC^4, compared with those of previous studies. Colors indicate approximate wind speeds in the upper troposphere.

Figure 8: . LIS (a) flash rate density (flashes km^{-2} s^{-1}) and (b) event rate density (events km^{-2} s^{-1}), gridded in $0.1^o \times 0.1^o$, prior to the OMI overpass, on the July, 21, 2007 case. The light gray shaded area corresponds to LIS field of view during this orbit passage. Frequency of occurrence of flash footprints during LIS observations of (c) the July, 21, 2007 case, and (d) 2007 boreal summer (June, July, August – JJA).

Tables

Table 1: Summary of LNO_x measurement results.

Date	Region	Area (10^3 km^2)	300 hPa Winds (Direction, m/s)	LNO_x (kmol)	Lightning Flashes	P_{IC+CG} (mol/flash)
July 17	South of Panama/CR	160	ENE 4	907	4931	184 ±285
July 21	NW coast of Colombia	194	W 2 (north side) E 2 (south side)	2972	20515	145 ±132
July 31	SW of Costa Rica	478	E 8	9022	14190	636 ±372
August 5	W coast of Colombia	246	NE 14	4572	10388	430 ±304

Table 2a: LNO_x in each region and contributions to the error budget.

Date	Value (kmol)	Random Error (kmol)	Systematic Strat,Trop Error (kmol)	Region-selection Error (kmol)	Combined Error (kmol)
July 17	907	±402	±1291	±205	±1367
July 21	2972	±525	±2409	±344	±2491
July 31	9022	±756	±4493	±2303	±5105
August 5	4472	±497	±2319	±1336	±2722

Table 2b: LNO_x and flash-count errors and their contribution to production-efficiency error.

Date	LNO_x (kmol)	Lightning Flashes (IC + CG)	LNO_x Production P_{IC+CG} (mol/flash)
July 17	907 ± 1367	4931 ± 1775	184 ± 285
July 21	2972 ± 2491	20515 ± 7385	145 ± 132
July 31	9022 ± 5105	14190 ± 2129	636 ± 372
August 5	4572 ± 2722	10388 ± 3740	430 ± 304

Table 3: Lightning NO_x enhancement factors

Date	NO_x (pptv) DC-8 in-cloud	NO_x (pptv) DC-8 clear sky	Enhancement Factor	OMI LNO_x. (10^{15} cm^{-2})	NO_x Background (10^{15} cm^{-2})	Enhancement Factor
July 17	110	60*	1.83	0.318 ± 1.099	0.743 ±0.159	1.43
July 21	538	309	1.74	0.860 ± 1.507	1.434 ± 0.275	1.60
July 31	876	375	2.34	1.275 ± 1.408	1.157 ± 0.356	2.10
Aug 5	357	152	2.35	1.052 ± 1.473	0.921 ± 0.155	2.14

*Taken from GMI model because of a lack of clear-sky observations unaffected by storm outflow or pollution plumes

Figures

Figure 1

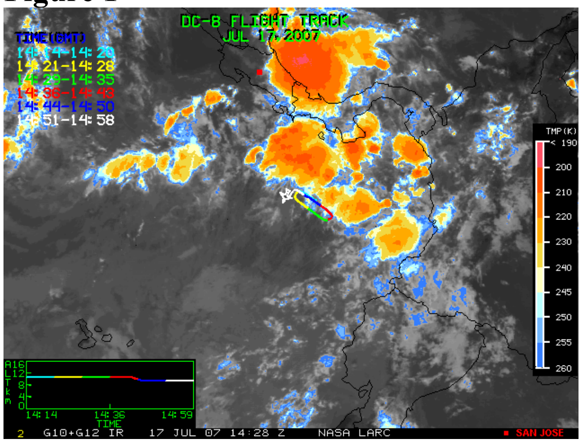

(a)

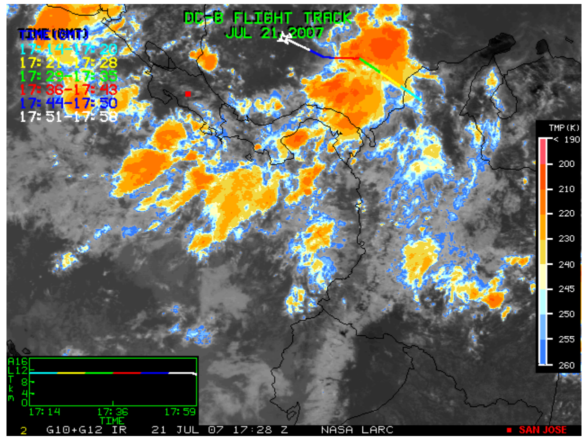

(b)

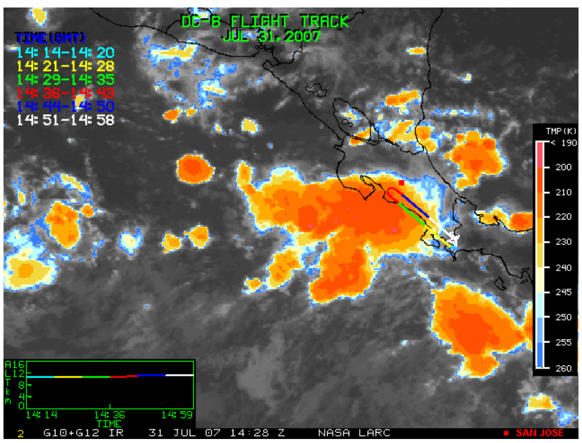

(c)

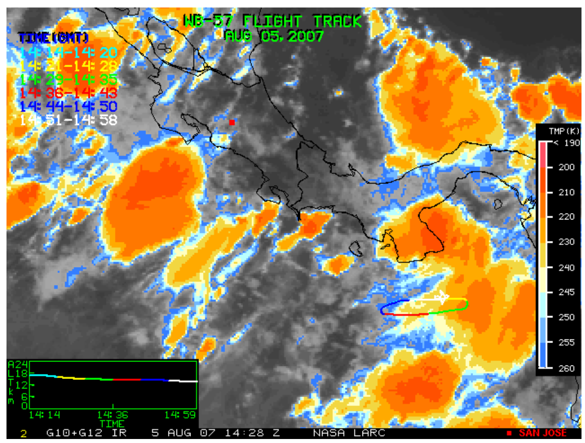

(d)

Figure 2

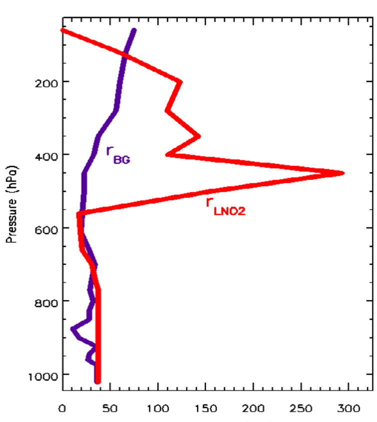

(a)

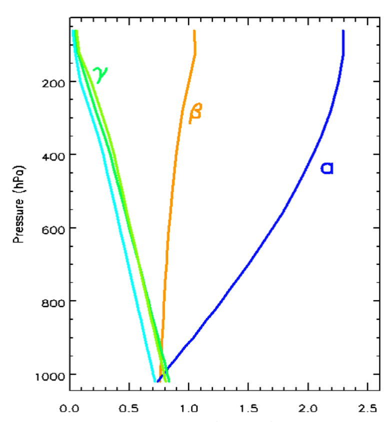

(b)

Figure 3

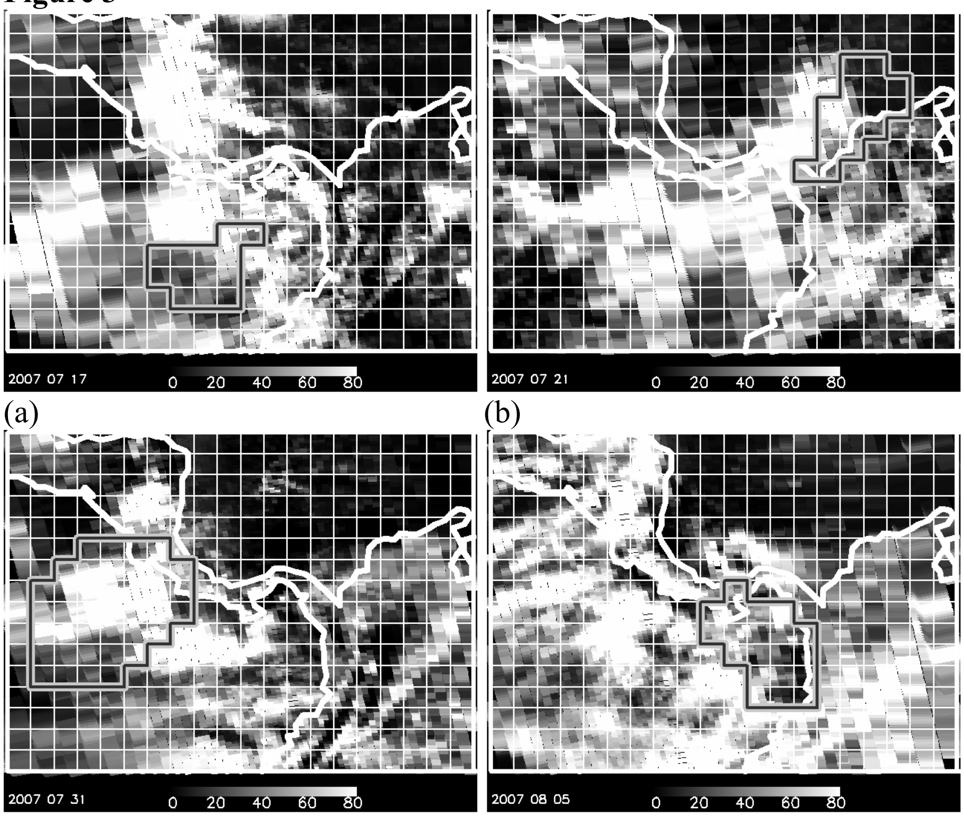

(a) (b)

(c) (d)

Figure 4

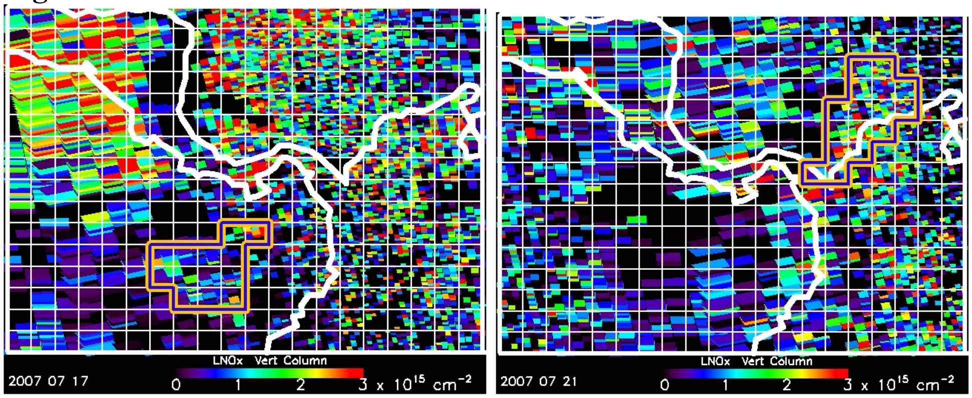

(a) (b)

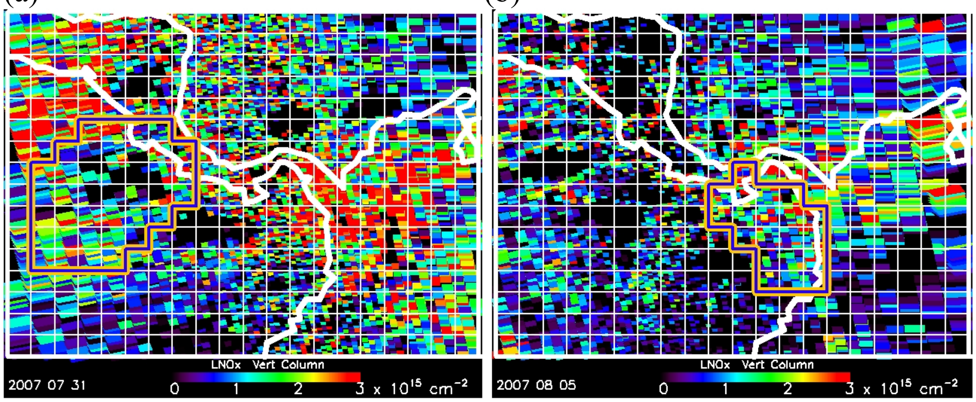

(c) (d)

Figure 5

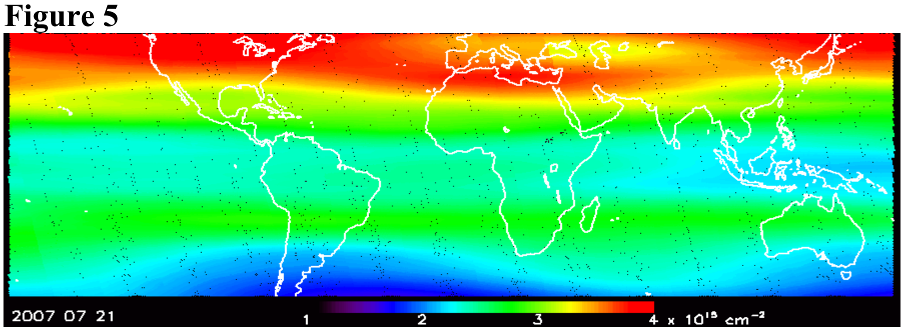

(a)

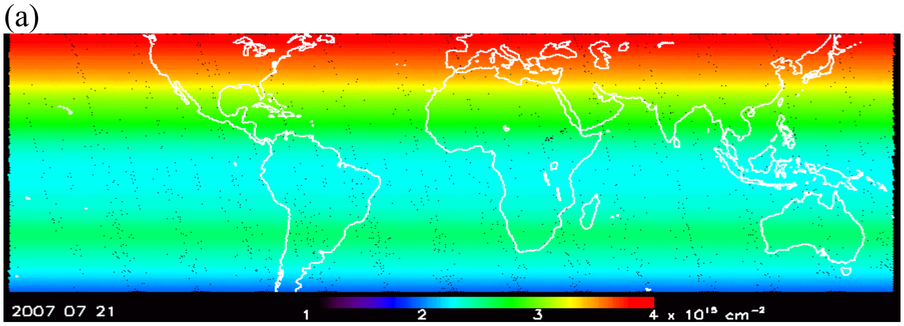

(b)

Figure 6

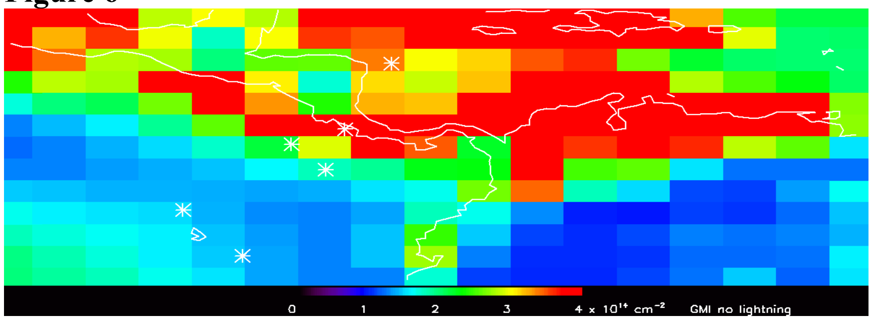

Figure 7

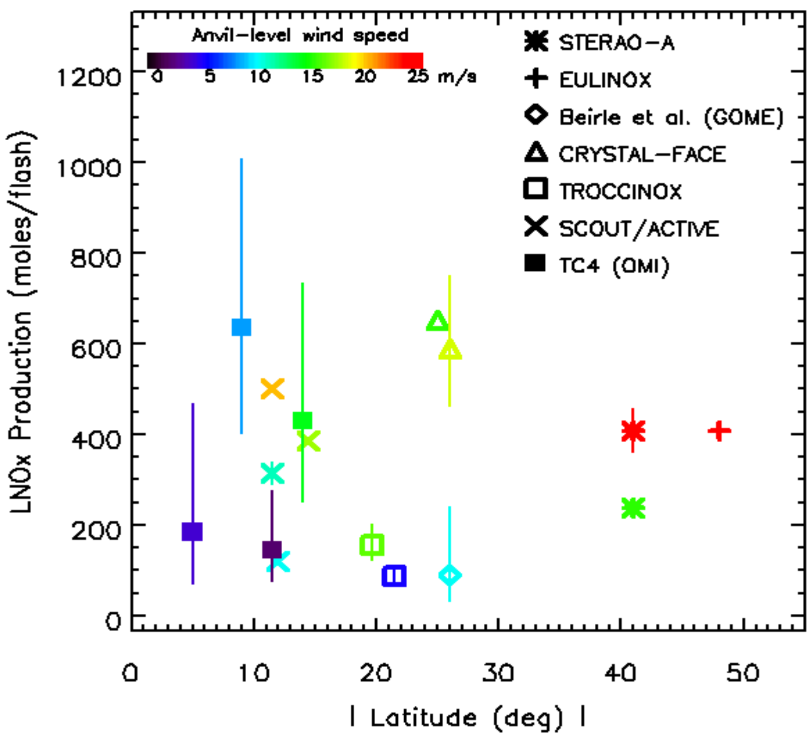

Figure 8

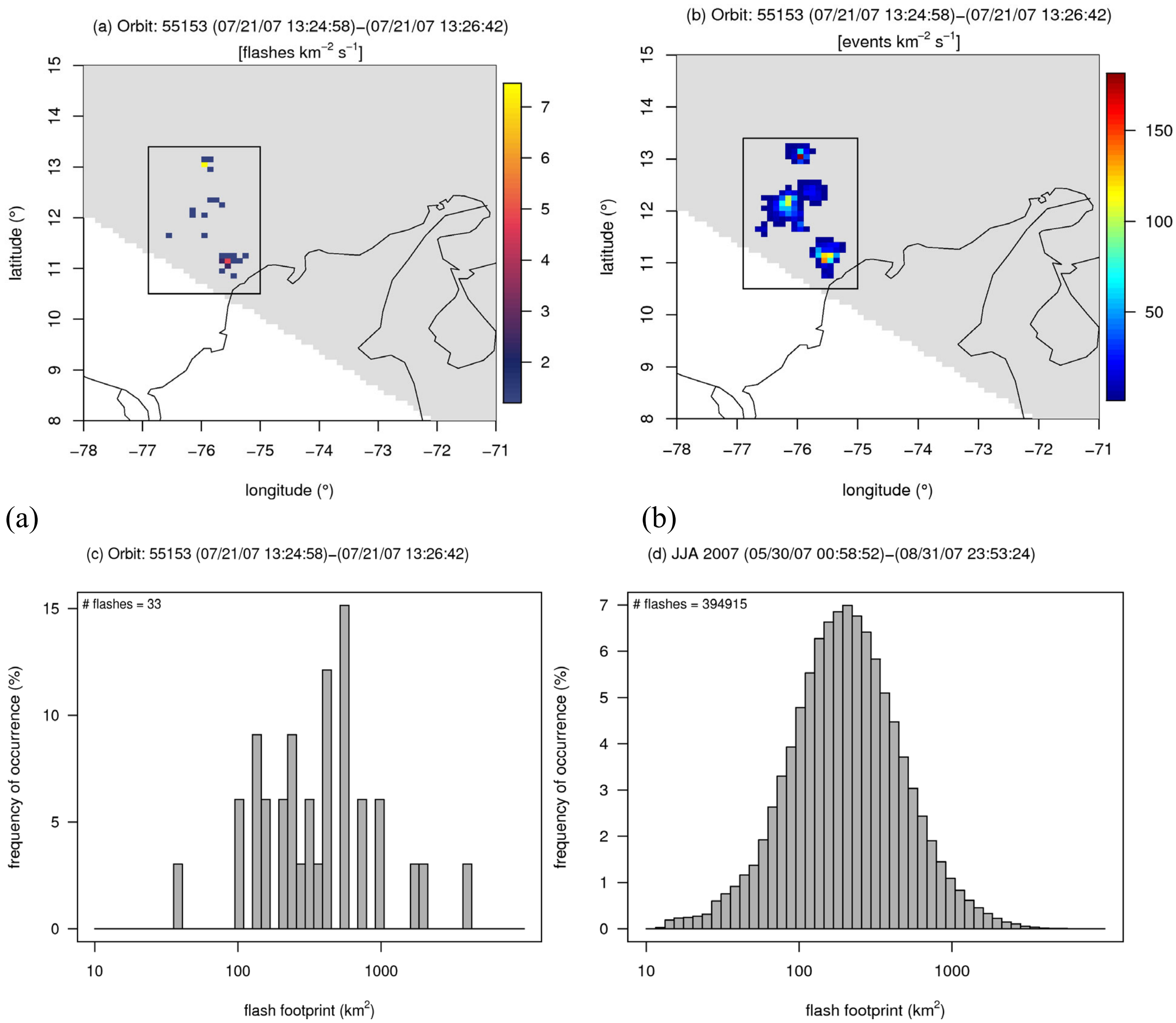

(a) Orbit: 55153 (07/21/07 13:24:58)–(07/21/07 13:26:42)
[flashes km^{-2} s^{-1}]
latitude (°)
longitude (°)
(a)
(b) Orbit: 55153 (07/21/07 13:24:58)–(07/21/07 13:26:42)
[events km^{-2} s^{-1}]
latitude (°)
longitude (°)
(b)
(c) Orbit: 55153 (07/21/07 13:24:58)–(07/21/07 13:26:42)
flashes = 33
frequency of occurrence (%)
flash footprint (km^2)
(d) JJA 2007 (05/30/07 00:58:52)–(08/31/07 23:53:24)
flashes = 394915
frequency of occurrence (%)
flash footprint (km^2)

(c) (d)